Toward the Confirmation of an Ultra-Short Period Hot Jupiter "Puffy Planet" with a Near Grazing Transit, TOI-2341.01

Darcy Wenn
Oscar Geerts
Derrick Liu
ELTHAM College of Education, 1660 Main Road, Research, VIC 3095, Australia; dtwenn@bigpond.com; oscargeerts@gmail.com; dliu40207@gmail.com

Michael Fitzgerald
Las Cumbres Observatory, 6740 Cortona Drive, Goleta, CA 93117; psyfitz@gmail.com

Saeed Salimpour
Max Planck Institute for Astronomy, Königstuhl 17, 69117 Heidelberg, Germany; IAU Office of Astronomy for Education, 69117 Heidelberg, Germany; Deakin University, 221 Burwood Hwy, Burwood, VIC 3125, Australia; astrophysics@saeedsalimpour.com

Andrew Yen
ELTHAM College of Education, 1660 Main Road, Research, VIC 3095, Australia; ayen@ELTHAMcollege.vic.edu.au

Received March 18, 2022; revisedAugust 11, 2022; accepted September 7, 2022

Abstract This paper reports on ground-based observations of the candidate exoplanet TOI-2341.01 (TESS Object of Interest-2341.01), initially observed by the Transiting Exoplanet Survey Satellite (TESS). The analysis of data provides evidence for the increased likelihood that TOI-2341.01 is a Jupiter-sized gas giant with a radius of 86,409 km ± 6,011 km (R_{Jup} 1.209 ± R_{Jup} 0.084), orbiting the host star TOI-2341 at 0.0118 AU ± 0.00073 AU with a transit duration of 0.065 days ± 0.006 days (1.560 ± 0.144 hours or 93.6 minutes ± 7 minutes). TOI-2341.01 has an orbital period of 0.877640 days ± 0.000004 day (21.0634 hours ± 0.0002 hour) and has a mid-transit time of BJD_TDB 2459411.74201 ± 0.00010. Furthermore, a grazing criterion value of 0.99 ± 0.14 was calculated, determining that TOI-2341.01 is highly likely to be a near-grazing transit. It is also noted that estimated mass values were attained via the TESS Follow-up Observation Program, projecting TOI-2341.01's mass as 55.3 M_E (0.17 M_J) and thus possessing an estimated density of 122.28 kg/m^3 (0.12228 g/cm^3). This investigation has also cleared the field surrounding TOI-2341.01 out to 43 arcminutes of eclipsing binaries that could produce a false positive.

1. Introduction

Over recent decades, exoplanet detection has increased exponentially, owing to space-based missions such as Kepler (Borucki *et al.* 2010) and TESS (Ricker *et al.* 2015). Although many detection methods such as radial velocity, microlensing, direct imaging, and transit timing variations are employed to determine the planetary systems of other stars, these aforementioned space-based missions have permitted the mass employment of the transit method, allowing for rapid, repeatable, and increasingly numerous exoplanet detections. This detection method requires stars to be monitored for drops in flux caused by a planet transiting in front of the star. The dip in flux allows for the determination of the planet's radius, orbital period, and semi-major axis. Since the launch of NASA's now-retired Kepler mission and current TESS mission, a new set of planetary objects has been discovered, dubbed "hot Jupiters." These planets have similar physical properties to Jupiter but have lower densities, are often tidally locked (Mandushev *et al.* 2007) and have extremely short orbital periods (usually less than ten days) with low eccentricities (Wang *et al.* 2015). Since its launch, NASA's TESS satellite has detected over 5,908 exoplanets to date; however, only about 4% of those have been confirmed, leaving many candidates to be investigated.

Table 1. Summary of each light curve quality and the definition of the assigned designations.

Light Curve Quality	*Definition*
Good Light Curve	Light curves with a clear and complete drop in flux. The transit is easily visible and can be identified in residuals.
Poor Light Curve	Light curves clear and complete drops in flux but with undesirable properties such as minimal, unclear or noisy drops in flux despite otherwise favourable atmospheric conditions.
Partial Light Curve	Light curves cut off on either side of the transit due to atmospheric conditions such as cloud, rain, wind or light.
Technical Issues	Light curves that produced an error while being processed due to weather, image error, insufficient data or other anomalies.

Under this premise, the investigation of exoplanet candidate TOI-2341.01 (TOI-2341 b) commenced. This investigation aims to highlight this exoplanet candidate's properties and nature to understand this planetary body further and add to the ever-increasing catalogue of previously discovered hot Jupiter class exoplanets. Prior to this investigation, TOI-2341.01 was characterized by TESS and associated surveys to possess a semi-major axis relative to stellar radius ratio (a/R_s) of 4.641 ± 1.021

Table 2. Details of observations.

Light Curve Designation TOI2341.01	*Date of Observation (MM/DD/YYYY)*	*Telescope*	*Observatory*	*Filter*	*Exposure Time (seconds)*	*Detrending Parameter*	*Transit Quality*
ECB.1	08/26/2021	PlaneWave Instr. CDK 17"	ELTHAM College	Bessel B	180	0.967664421	Partial
ECIP.1	09/08/2021	PlaneWave Instr. CDK 17"	ELTHAM College	SDSS i'	240	0.997830786	Partial
ECL.1	09/16/2021	PlaneWave Instr. CDK 17"	ELTHAM College	Luminance	240	1.00163253	Good
ECL.2	09/23/2021	PlaneWave Instr. CDK 17"	ELTHAM College	Luminance	40	1.006906109	Good
ECL.3	09/25/2021	PlaneWave Instr. CDK 17"	ELTHAM College	Luminance	40	1.002733981	Technical error
ECL.4	09/26/2021	PlaneWave Instr. CDK 17"	ELTHAM College	Luminance	40	1.001186931	Poor
ECRP.1	09/01/2021	PlaneWave Instr. CDK 17"	ELTHAM College	SDSS r'	180	0.999270846	Partial
ECRP.2	08/19/2021	PlaneWave Instr. CDK 17"	ELTHAM College	SDSS r'	90	0.99475672	Partial
LCOB.1	10/04/2021	Meade LX200 16"	Cerro Tololo	Bessel B	90	1.006974028	Technical error
LCOB.2	09/05/2021	Meade LX200 16"	Cerro Tololo	Bessel B	300	1.02133523	Poor
LCOIP.1	09/24/2021	Meade LX200 16"	Siding Springs	SDSS i'	90	1.007174333	Good
LCOIP.2	09/02/2021	Meade LX200 16"	Siding Springs	SDSS i'	300	1.009928858	Partial
LCOIP.3	09/09/2021	Meade LX200 16"	Siding Springs	SDSS i'	300	1.00223799	Good
LCORP.1	09/05/2021	Meade LX200 16"	Cerro Tololo	SDSS r'	300	1.002108894	Poor
LCORP.2	10/04/2021	Meade LX200 16"	Cerro Tololo	SDSS r'	90	0.999053465	Good
LCOV.1	09/26/2021	Meade LX200 16"	Cerro Tololo	Bessel V	90	1.018566403	Good
LCOW.1	07/01/2021	Meade LX200 16"	Cerro Tololo	Pan-STARRS w	75	1.008050852	Partial
LCOW.2	07/17/2021	Meade LX200 16"	Cerro Tololo	Pan-STARRS w	75	1.014530207	Good
LCOW.3	07/16/2021	Meade LX200 16"	Cerro Tololo	Pan-STARRS w	75	1.025370914	Good
LCOW.4	09/24/2021	Meade LX200 16"	Siding Springs	Pan-STARRS w	40	1.006302628	Poor
LCOW.5	09/24/2021	Meade LX200 16"	Siding Springs	Pan-STARRS w	40	1.00176371	Partial
LCOW.6	09/23/2021	Meade LX200 16"	Siding Springs	Pan-STARRS w	40	1.00112731	Technical error
LCOZS.1	10/08/2021	Meade LX200 16"	Siding Springs	Pan-STARRS Zs	90	1.013713456	Good
LCOZS.2	09/09/2021	Meade LX200 16"	Siding Springs	Pan-STARRS Zs	300	1.004841398	Good

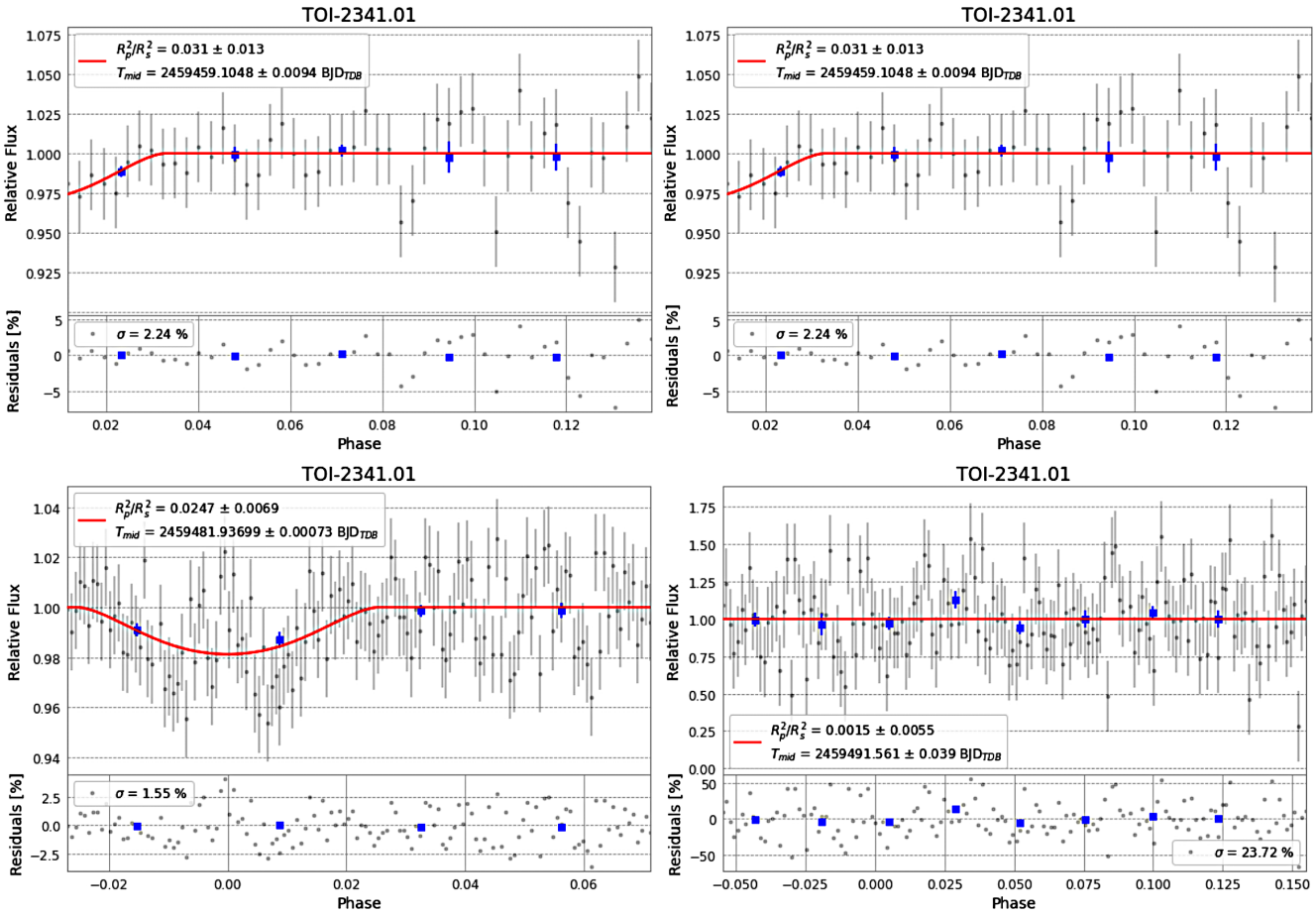

Figure 1. The top left panel is an example of a "Partial Light Curve," as a portion of the transit is missing from the graph. The top right panel is an example of a "Good Light Curve"; a clear and pronounced drop in stellar flux is shown. The bottom left panel is an example of a "Poor Light Curve," as noise drastically affects the transit plot and residuals. The bottom right panel is a "Technical Issue"; despite taking place in the transit window, no transit is shown.

and a ratio of planetary radius to the stellar radius (R_p/R_s) of 0.097 ± 0.008 (Montalto *et al.* 2020).

2. Observations

Observations of 24 transits of TOI-2341.01, collected between 1 July 2021 and 4 October 2021, were analyzed. These observations were conducted at the ELTHAM College Observatory utilizing a PlaneWave Instruments CDK 17-inch (0.43-m) telescope equipped with an SBIG STX-16803 CCD camera giving a field of view of 43.12 × 43.12 arcminutes, and on the Las Cumbres Observatory (LCO) Network (Brown *et al.* 2013), utilizing the Meade LX200 16-inch (0.4-m) telescopes equipped with SBIG STL-6303 CCD cameras giving a field of view of 29.2 × 19.5 arcminutes. All data were captured from the ELTHAM College Observatory in Victoria, Australia, the Siding Springs Observatory in New South Wales, Australia, and the Cerro Tololo Inter-American Observatory in Chile's Coquimbo Region. The observations on the LCO network were scheduled using ExoRequest (Sarva *et al.* 2020; Salimpour *et al.* 2021).

3. Data quality

To attain satisfactory data for the production of a light curve, several environmental factors must be considered, such as lack of cloud cover, accurate telescopic tracking, a minimal field of view (FOV) drift, and good seeing (sharp images due to still stratospheric and mesospheric conditions). Seeing significantly affected many of the later transits collected for this investigation due to TOI-2341.01's right ascension (R.A.) and thus low altitude in the southern sky during the observing campaign. Out of 24 transits in this study, 10 were "good transits." Each transit was given a designation denoting its quality, as explained in Table 1. A breakdown of the results from processing each transit is shown in Table 2, including the date of observation, the telescope and observatory utilized, filter, exposure time, and a column to indicate transit quality. Examples for each designation are shown in Figure 1. All light curves are shown in Appendix A.

4. Data reduction and light curve production

For photometric evaluation of the data, PSFEx (Point Spread Function Extractor; Bertin 2011) photometry, produced by the OSS (Our Solar Siblings) pipeline (Fitzgerald 2018), was analyzed through the Python script Astrosource (Fitzgerald *et al.* 2021), which used ensemble photometry to produce a series of output files and plots containing the variability in flux seen from TOI-2341 during the transit period. Astrosource also created a list of calibration stars for utilization in the production of a transit curve. Comma Separated Value (.csv) output files measuring the barycentric dynamical time (BJD_TDB), orbital phase, and flux produced by Astrosource were subsequently input into the EXOTIC (EXOplanet Transit Interpretation Code) pipeline (Zellem *et al.* 2020). The selected comparison stars are listed in Table 3 and shown in Figure 2, and were set to be close to the target, not too close to other stars in the field, and sufficiently bright. These comparison stars were used as an ensemble by Astrosource to extract the exoplanet light curves.

Table 3. Comparison stars selected by Astrosource.

Letter Designation	*Star Name*
B	TYC 8790-2326245
C	HD 194254
D	UCAC2 8922690
E	AAVSO 035-3704842
F	AAVSO 035-2326245
G	UCAC3 74-468439

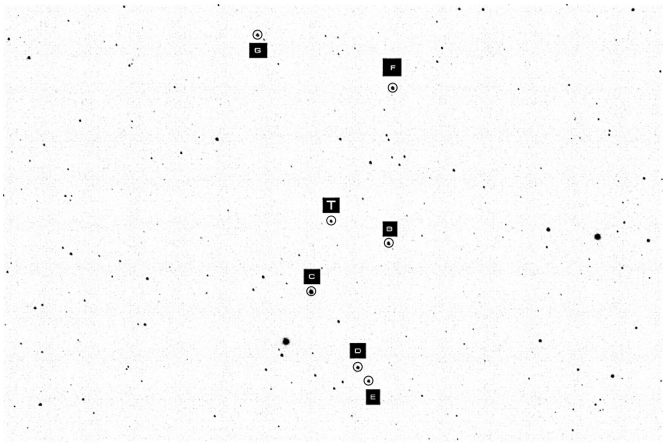

Figure 2. An image of the target star, TOI-2341 (label T), and the comparison stars (listed in Table 3) that were automatically selected by Astrosource.

The EXOTIC software was run via Python 3.10 across versions 1.0 through 1.10. The parameters of TOI-2341.01 provided from the NASA Exoplanet Archive (NEA), details of the imaging session, and the telescope utilized for each session were entered into JavaScript Object Notation (.json) files, which were utilized by the EXOTIC pipeline.

EXOTIC was then used to perform an MCMC (Markov-Chain Monte Carlo) fitting routine to fit an exoplanet transit model to the reduced light curve, as shown in Figure 3. EXOTIC also reports from this fit the scatter in the residuals, the mid-transit time (T_{mid}), transit depth $(R_p/R_s)^2$, the ratio of planetary radius to the stellar radius (R_p/R_s), semi-major axis relative to the stellar radius (a/R_s), air mass, and transit duration (T_{dur}) throughout the observation window.

Furthermore, EXOTIC detrends data pertaining to the production of a light curve by fitting to the function defined in Equation 1, where c is the coefficient to which the data are fitted, and airmass is the actual air mass value for that respective dataset as determined by EXOTIC and telescope data.

$$f = e(c \times \text{airmass}) \quad (1)$$

Detrending values for each transit are listed as part of Table 2.

4.1. EXOTIC data and analysis

Astrosource and EXOTIC's reduction processes produced 24 new light curves of TOI-2341.01, shown in Appendix A. Each light curve shows the measured normalized flux over the transit period, with some datasets comprising larger portions of the orbital phase than others. Error bars are also included for each plot point during transit and non-transit periods.

Table 4. Parameters produced by EXOTIC reduction.

Planetary Parameters	*Value*	*SEM*	*Error (%)*
Ratio of planet to stellar radius (R_p/R_s)	0.20033	± 0.01393	6.96
Transit depth (R_p/R_s)	4.191	± 0.528	12.61
Semi major axis/stellar radius (a/R_s)	4.1079	± 0.2542	6.19
Scatter in the residuals of the lightcurve fit	1.757	± 0.312	17.77
Transit duration	0.065	± 0.006	9.26

The resulting plot shows relative flux over phase, and a trendline of the light curve is overlaid. Residuals are also stated under the primary graph, and $(R_p/R_s)^2$ (transit depth) and the Tmid (transit midpoint) are shown overlaid on the primary graph. EXOTIC also outputs planetary parameters in the format of a .txt file, stating the (R_p/R_s), (a/R_s), transit depth $(R_p/R_s)^2$, and transit duration (T_{dur}).

To assess the reliability of planetary parameters while using a complete dataset, an "outlier clipping" algorithm was performed. This algorithm compares a given parameter across all inputted transits and eliminates all values that deviate substantially from the mean. In particular, all values with a distance greater than twice the standard deviation from the mean are discarded. It is noteworthy to mention the recursive nature of this algorithm; if a value is clipped, the standard deviation is recalculated, and the algorithm resets until no clips are recorded. Following the removal of outliers, the mean and standard error are calculated and are respectively displayed as planetary parameter ± error.

The planetary parameters seen in Table 4 are outputted from this algorithm making use of data derived from all ten "good" transits. The algorithm did not clip any values from any of the transits inputted, indicating a high degree of data consistency across the "good" transits.

In some instances, the values presented in this investigation deviate compared to previous literature (Montalto *et al.* 2020). The transit depth has been determined to have increased from prior literature from 1.205% ± 0.003% to 4.191% ± 0.529%. The semi-major axis over stellar radius (a/Rs) has decreased relative to previous literature from 4.64 ± 1.02 to a value of 4.108 ± 0.254.

The Transit Duration (days) of TOI-2341.01 has increased from 0.019 ± 0.055 to 0.065 ± 0.006, approximately three times the value published by the NASA Exoplanet Archive. The increase in Tdur likely results from how EXOTIC measures transit duration. However, this value is precise and accurate. A gradual sloping transit occurs between phases –0.04 and +0.04; this may be attributed to the near grazing nature of TOI-2341.01's transit. The 0.08 phase between these points is equivalent to the calculated transit duration and can be observed in Figure 3.

The planet-to-stellar radius (R_p/R_s) ratio is noted to have increased from 0.097 ± 0.008 to 0.200 ± 0.014. This investigation has determined that TOI-2341.01 has a radius of roughly 20.03% ± 0.19% of its host star, TOI-2341, as determined by the aforementioned (R_p/R_s) value. TOI-2341 is likely to be an M-type main-sequence star. This classification is based on TOI-2341's radius of 0.62 $R_\odot$ ± 0.02 $R_\odot$, an effective temperature of 3495 K ± 157 K, and a measured magnitude of 12.722 ± 0.008

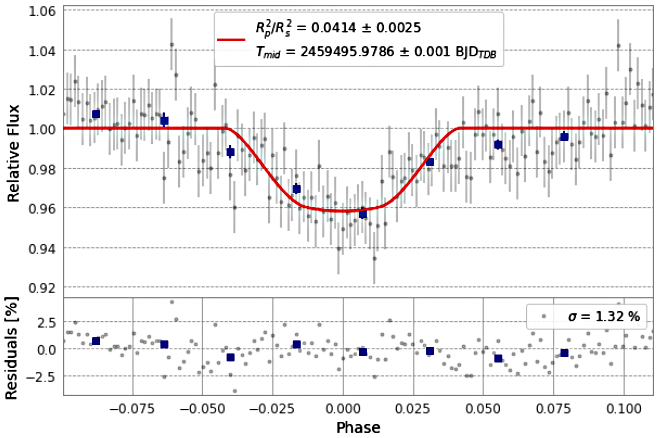

Figure 3. A light curve produced from an imaging session conducted on the Las Cumbres Observatory Network using a ZS filter (Effective central wavelength 870 nm, Full Width at Half Maximum 104 nm). Here a clear drop in relative flux is demonstrated, outlining the transit of TOI-2341.01.

utilizing TESS's detector bandpass of 600–1000 nm centered on the Cousins I band with a wavelength of 786.5 nm (Barclay 2022) . The luminosity of TOI-2341.01 was calculated to be 0.0514 ± 0.006, as given by the Stefan-Boltzmann equation for luminosity seen in Equation 2. Furthermore, the TESS Follow-up Observation Program (TFOP) lists an estimated mass for TOI-2341 as 0.6 $M_\odot$. These characteristics match with known properties of M-type stars, and values for calculation were provided by available literature of TOI-2341 from the NASA Exoplanet Archive and Montalto *et al.* (2020).

$$L = 4\pi R^2 \cdot \sigma T^4 \quad (2)$$

The Stefan-Boltzmann Law (Equation 2): In this equation, σ is the Stefan-Boltzmann Constant where $\sigma = 5.67^{-8}$ $(W/(m^2 \times K^4))$.

From the R_p/R_s value stated above, the planetary radius of TOI-2341.01 can be determined. The value for R_s was used from the NASA Exoplanet Archive, 0.62 ± 0.02 $R_\odot$. The formula for calculating planetary radius (r_{km}) is shown in Equation 3.

$$r_{km} = R_s \cdot (R_p / R_s) \pm SEM \quad (3)$$

Just as the planetary radius of an exoplanet can be calculated utilizing R_p/R_s, the semi-major axis of an exoplanet can be determined from the EXOTIC output a/R_s. The larger the semi-major axis, the longer the orbital and transit periods, which is how EXOTIC calculates this parameter when calculating an individual light curve. The equation utilized is shown in Equation 4.

$$d_{AU} = \frac{R_s \cdot (a / R_S)}{1.496 \cdot 10^8 \text{ km}} \cdot 1AU \pm \frac{SEM}{1.496 \cdot 10^8 \text{ km}} \cdot 1AU \quad (4)$$

Equations 3 and 4 and their respective SEM (standard error to the mean) calculations were performed for each "good transit" dataset, leading to an average value from 10 data points in combination with the SEM. These results are reported in AU and km to align with the prior literature; however, comparison values are also stated. The planetary radius of TOI-2341.01 is

calculated to be approximately 86,409 km ± 6011 km, or 1.209 ± 0.084 R_{Jup}. The semi-major axis of TOI-2341.01 was calculated to be approximately 0.0118 AU ± 0.0007 AU. Directly related to the semi-major axis, the transit duration of TOI-2341.01 was determined by EXOTIC to be 0.065 day ± 0.006 day (1.560 ± 0.144 hours or 93.6 ± 8.6 minutes). The calculated radius value falls outside the uncertainty values presented within the NASA Exoplanet Archive and prior literature (Montalto *et al.* 2020). In this investigation, it has been calculated that TOI-2341.01 is approximately 63% larger than previously calculated, a difference of 4.95 Earth radii. However, we conclude that this increase in radius over previous calculations is likely to be closer to the true value due to the increased number of recorded transits, the near grazing nature of the TOI-2341.01 light curve, and the quality of the light curves used in the production of these parameters.

4.2. The ephemeris data and analysis

As part of EXOTIC's reduction process, a text file (.txt) of planetary parameters is produced. These .txt files include T_{mid} (mid-transit time) values for the reduced transit. To provide updated orbital period and Tmid values as part of this investigation, Tmid values from all 10 "good transits" were collated into a .csv file alongside the respective standard error to the mean values (SEM). The .csv file was accompanied by a JSON file containing the calculated parameters for TOI-2341.01 produced by EXOTIC. Following the production of both files, the .csv file was fed through an ephemeris fitter (Pearson 2019) that collated each Tmid value from the available transits and produced a revised transit midpoint and orbital period for TOI-2341.01. These values are noted in Table 5. A plot is also produced (Figure 4), revealing the deviation between each recorded mid-transit time from each observation and the predicted mid-transit time derived from the ephemeris fitter's new transit midpointvalue. Below that plot, a residuals plot is shown, demonstrating the deviation of each recorded mid-transit time from the calculated transit midpoint value in minutes. It is noted that the values presented are confirmed as precise due to the repeated observation of TOI-2341.01 over multiple months.

It is also noted as part of this investigation that a test run of the ephemeris fitter was performed that included all 24 transits in the production of an updated ephemeris for TOI-2341.01. This test resulted in very similar values for orbital period and transit midpoint, with slightly greater error values produced that overall did not deviate from the dataset provided in this publication. It was ultimately decided to use the "good transits" only to maintain consistency with the planetary parameters for TOI-2341.01 calculated using only that portion of the dataset.

4.3. The near grazing nature of TOI-2341.01

It can also be stated, based on the nature of the transit plots produced by EXOTIC, that it is a possibility that TOI-2341.01 is a near grazing transit. In a traditional grazing transit, such as WASP-67b (Mancini *et al.* 2014), the second and third contact points where the planetary body has entirely passed in front of the stellar disk are missing from the transit light curve. In essence, a grazing transit is where the planet skims or only partially occludes the stellar disk, leading to a "v-shaped" or

Table 5. Revised orbital period and transit midpoint values calculated via the ephemeris fitter and their respective errors.

Parameter	*Value*	*SEM*
Orbital period (days)	0.877638	± 0.000004
Transit midpoint (BJD_TDB)	2459411.742011	± 0.000131

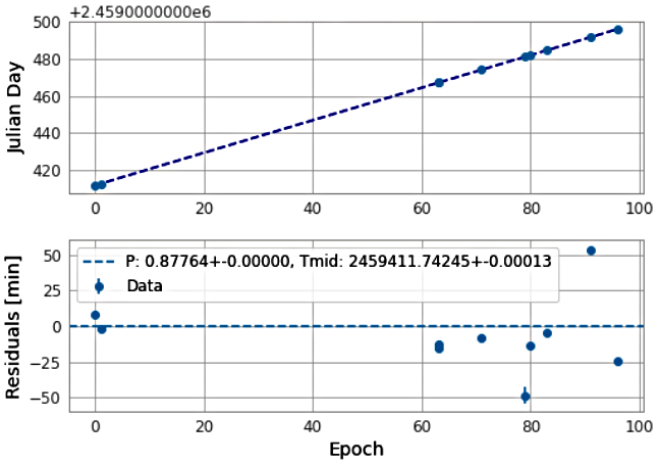

Figure 4. A plot of the deviation between each recorded mid-transit time from each observation and the predicted mid-transit time derived from the ephemeris fitter's new transit midpoint value.

shallow light curve instead of a standard, flat-bottomed light curve. As shown in Figure 5, TOI-2341.01 exhibits similar characteristics to HAT-P-14b (Torres *et al.* 2010), a grazing transit, in contrast to another Hot Jupiter, HAT-P-32b (Hartman *et al.* 2011), which is a regular transit. Furthermore, TOI-2341.01 is listed in prior literature as a v-shaped, potentially grazing transit with an orbital inclination of 78.93° ± 2.02° (Montalto *et al.* 2020). As 0° represents the planet passing directly between Earth and the relevant star, and 90° represents an "edge-on" orbit relative to Earth, it is noted that 78.93° is an extremely high orbital inclination and therefore likely to only partially occlude TOI-2341. The grazing criterion can be calculated to determine whether a planet is a grazing transit (Lillo-Box *et al.* 2015). To calculate the grazing criterion, one must calculate the impact parameter (b) using Equation 5.

$$b = \frac{a \cos i}{R_*} \quad (5)$$

Solving for a in ratio $a/R_s = 4.1079$ results in a value of a = 2.53523. The value a is defined as the semi-major axis of TOI-2341.01. Using Equation 5, the value of b is calculated to be 0.79 ± 0.14. Therefore, when calculating the grazing criterion, the ratio $R_p/R_s = 0.2003 \pm 0.0139$ and the impact parameter b = 0.79 ± 0.14 suggest that TOI-2341.01 is likely to be a near grazing transit. For a transit to be grazing, a value of > 1 must be calculated using Equation 6.

$$b + R_p / R_S > 1 \quad (6)$$

For TOI-2341.01, a value of 0.99 ± 0.14 is calculated, creating an upper value of 1.13 and a lower value of 0.85 for the grazing criterion. As the calculated grazing criterion for TOI-2341.01 is 0.99 ± 0.14, and a grazing transit is considered any value > 1,

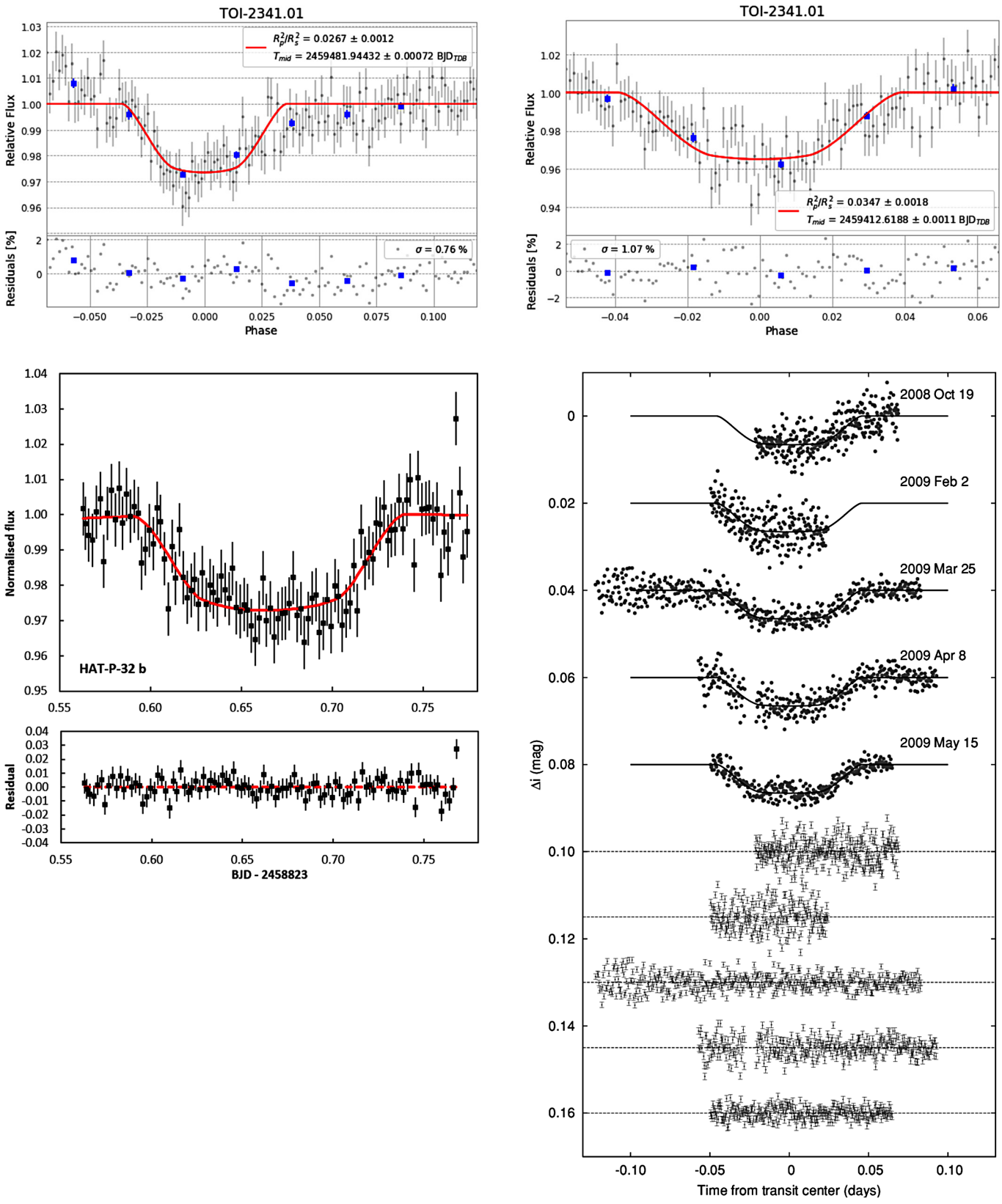

Figure 5. Examples of TOI-2341.01 transit plots during this investigation (top row) compared to HAT-P-14b (Torres *et al.* 2010) (right) and HAT-P-32b (Fowler *et al.* 2021) (bottom left). Note the similarities between HAT-P-14b's and TOI-2341.01's near grazing transit. The similarity is demonstrated in trend lines and flux plots that follow a smoother curve that does not define a transit bottom clearly. Compared to HAT-P-32b's complete occlusion and flat-bottomed transit, the flux plots and a sharper transit curve are demonstrated.

TOI-2341.01 is likely a near grazing transit. Therefore, it is similar to near-grazing transits like that of HAT-P-14b, which has a grazing criterion of 0.968 ±0.022.

The categorization of TOI-2341.01 as a near grazing transit is also concluded from the light curves produced. Traditional light curves will show a significant, rapid drop in stellar flux during the transit period, with a steep and equal curve in the final minutes of the transit period. For near-grazing or grazing transits, an observed transit and its subsequent light curves will show shallow, slow drops in stellar flux that are evidence of a grazing nature of a planet. Examples of the difference between a standard and near grazing transit light curve plot, including a comparison to TOI-2341.01, are shown in Figure 5.

4.4. The estimated mass of TOI-2341.01

While radial velocity measurements have not been recorded for TOI-2341.01 as of the writing of this publication, estimated mass measurements for TOI-2341 and TOI-2341.01 have been published on the TESS Follow-up Observing Program (TFOP) website. These estimations are provided in Table 6 (Massachusetts Institute of Technology (MIT) 2021).

It can therefore be stated for the purposes of this investigation that TOI-2341's assumed mass is 0.6 $M_{\odot}$ and TOI-2341.01's assumed mass is 55.3 M_E. It is important to note that these mass values are estimates based on available data supplied by TESS on the NASA Exoplanet Archive, TFOP (MIT 2021), and prior studies (Montalto *et al.* 2020). While these mass values cannot be used as substitutes for confirmed mass parameters determined through radial velocity measurements, these values have been checked for accuracy as visualised below.

Equation 7, Kepler's Third Law, can be utilized to calculate the orbital period of a planetary body, in this case TOI-2341.01.

$$T^2 = \frac{4\pi^2}{G \times (M_1 + M_2)} \times r^2 \quad (7)$$

In Kepler's Third Law, T is the orbital period in minutes, G is the gravitational constant (6.6743×10^{-11} m^3 kg^{-1} s^{-2}), M is the mass of an object in solar masses, and r is the radius of the satellite's orbit in astronomical units. If the calculation of an orbital period utilizing Kepler's Third Law and values provided from both this investigation and mass values from TFOP (MIT 2021) aligns with the calculated ephemerides as part of this investigation, then these mass estimates can be used to bolster this investigation's conclusion that TOI-2341.01 is indeed likely to be a strong planet candidate. Substituting the values into Equation 7 the formula looks as follows:

$$T^2 = \frac{4\pi^2}{(6.6743 \times 10^{-11}) \times (0.6 + (1.166051 \times 10^{-4})} \times 0.0118^2 \quad (8)$$

Solving for T, a value of 1272.57 minutes, just 8.76 minutes greater than the 1263.80-minute orbital period determined by the ephemeris fitter as part of this investigation. As the value established by Kepler's Third Law is 0.00688% greater than the value calculated by the fitter, the team has deemed these estimate mass values notable and in line with new values calculated in this investigation, giving greater plausibility to the likelihood of TOI-2341.01 being a strong planetary candidate. However, it should be stated again that these mass values are estimates provided by TFOP and should not be used over values provided by radial velocity measurements. Radial velocity measurements of TOI-2341.01 should be calculated in follow-up studies of this star system as outlined in section 8.

Table 6. Estimates of the mass of TOI-2341 and TOI-2341.01 provided by the Massachusetts Institute of Technology's TESS Follow-up Observation Program.

Stellar Body	*Estimated Mass ($M_{\odot}$)*	*Estimated Mass (M_J)*	*Estimated Mass (M_E)*
TOI-2341	0.6	628	333030
TOI-2341.01	1.66051×10^{-4}	0.173	55.3

4.5. Estimates of a low density "Puffy Planet"

Utilizing mass measurements from TFOP (MIT 2021) and radius measurements determined by EXOTIC, it is possible to estimate the density of TOI-2341.01 by determining the mass and volume of the planet. TFOP has listed TOI-2341.01's mass as 55.03 M_E, which is equivalent to 3.302516×10^{26} kg. This investigation has determined TOI-2341.01's radius to be 86,409.140 km ± 6011.210 km. Converting to meters, the new values are 86,409,140 m ± 60,1121 × 10^6 m. The volume of TOI-2341.01 can be determined with Equation 9:

$$\frac{4}{3} \times \pi \times 86409140^3 \quad (9)$$

This formula provides a value for TOI-2341.01's internal volume of 2.7025122×10^{24} m^3. By dividing the mass of TOI-2341.01 in kilograms by the volume in cubic meters as demonstrated in Equation 10, an estimate density value can be attained.

$$\frac{3.304728 \cdot 10^{26}}{2.7025122 \cdot 10^{24}} = 122.2835 \text{ kg/m}^3 \quad (10)$$

The calculated density estimates of 122.2835 kg/m^3 or 0.12228 g/cm^3 places TOI-2341.01 in the low mass, high radius range of hot Jupiter class exoplanets, also known as "Puffy Planets." While it is important to reiterate that these density and mass values are again estimates and should be followed up with prior study as detailed in section 8, these values add weight toward TOI-2341.01's likelihood of remaining a strong planetary candidate.

5. Blended eclipsing binaries and candidate legitimacy

A common false positive among TESS planet candidates is the presence of a "blended eclipsing binary" (EB). A blended EB occurs when another star and an orbiting planet or secondary star as part of a binary system exists close to the star being observed, in this case, TOI-2341, causing an erroneous signal similar to a planetary transit. Due to disparity in transit depth as a result of noise within the light curves collected by this investigation, a chromaticity check was undertaken to identify major deviations from a mean transit depth that could indicate a blended EB.

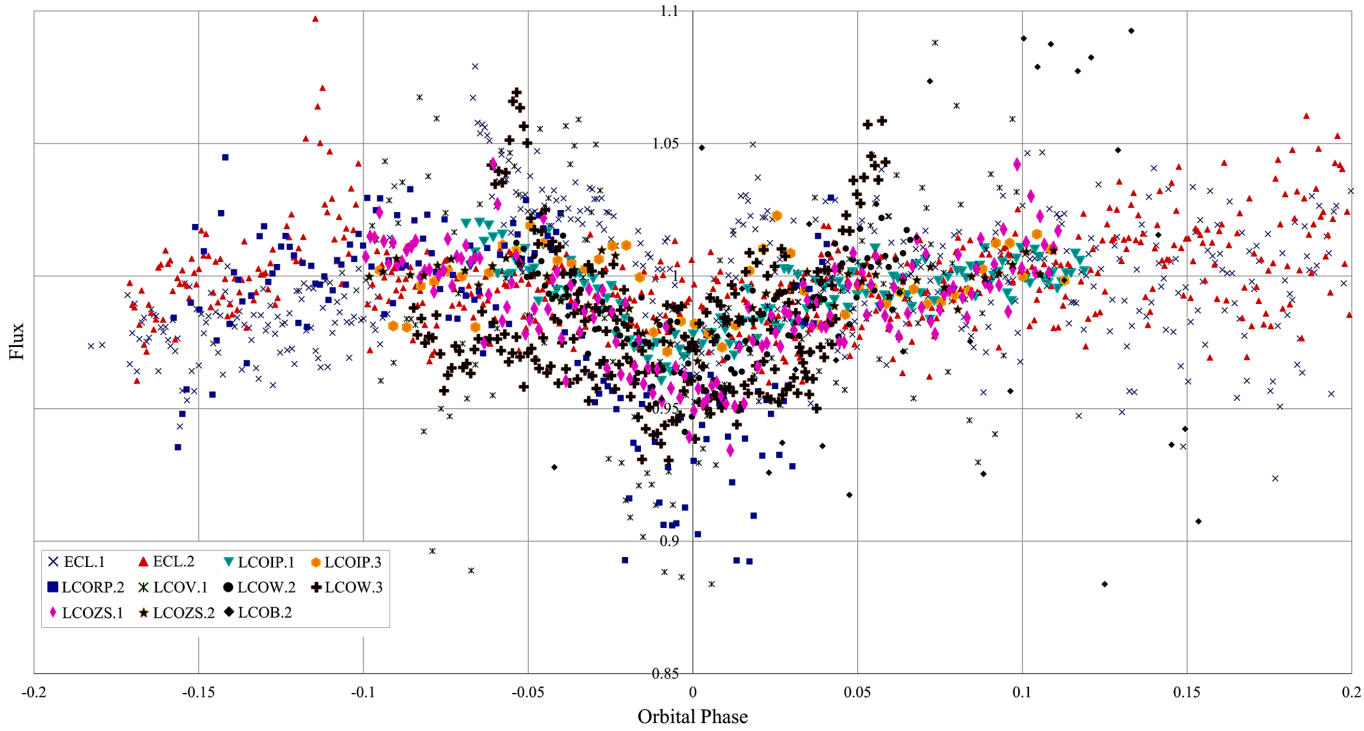

Figure 6. A visual demonstration of all ten "good transits" overlaid with "poor transit" TOI2341.01LCOB.2 to demonstrate deviation from the mean transit depth of 4.191 ± 0.529.

Blended EBs are also responsible for false "grazing-transit" detections, hence it was necessary to provide evidence to clear the observed field around TOI-2341 of blended and regular EBs. Table 7 presents recorded transit depths compared to the observed passbands of all ten "good transits" within this investigation, and one "poor" transit to cover the blue passband. Transit Depth 1 in Table 7 denotes the first light curve of that passband, and Transit Depth 2 is the second where applicable.

Figure 6 demonstrates the relationship between the ten "good transits" as well as a "poor" B Filter transit, TOI2341.01LCOB.2. Each transit does not significantly deviate from the mean transit depth of 4.191 ± 0.529 excluding the V and R passbands, of which there was only one recorded "good transit" and hence is the likely causation of its deviation.

Utilizing results provided by Table 7 and Figure 6, it can be stated that there is no correlation between different passbands and differing transit depths due to the high uncertainty values inclusive of the same passband across multiple transits. Therefore, it is likely differing transit depths across passbands can be attributed to noise caused by weather, equipment, or anomalies presented by the potential near grazing nature of TOI-2341.01 as illustrated in section 4.3.

Further evidence to clear the field of the TOI-2341 system of blended EBs can be found in prior literature where it is stated that TOI-2341.01 has an inclination of 78.93° ± 2.02° (Montalto *et al.* 2020), further backed by section 4.3 where TOI-2341.01's grazing criterion is calculated to be 0.99 ± 0.14, pushing the likelihood of TOI-2341.01's near grazing nature to an increased chance.

Another common feature of blended EB's is an erroneous second dip in flux caused by two orbiting stars in a binary pair. As shown in Figure 7 (Montalto *et al.* 2020), there are no recorded secondary dips in flux from TOI-2341 between phase –0.4 and 0.4, potentially ruling out the presence of a blended EB along the light curve, or at the least drastically reducing its probability.

Table 7. Passbands and transit depths of "good transits."

Filter	*Transit Depth 1 (%)*	*Transit Depth 2 (%)*
IP	2.67 ± 0.12	5.73 ± 0.54
R	6.21 ± 0.0057	N/A
V	5.93 ± 0.36	N/A
B	6.23 ± 3.73	6.06 ± 3.47
UV	4.14 ± 0.25	3.69 ± 0.78
Luminance	5.81 ± 0.56	1.27 ± 0.11
Clear	3.47 ± 0.18	2.99 ± 0.21

Greater evidence can be presented for the absence of blended and eclipsing binaries by the estimated mass and density values provided by a combination of TFOP (MIT 2021) and prerequisite values calculated as part of this investigation. The mass of TOI-2341.01 is estimated to be 55.3 M_E (0.1739 M_J) and its density is projected to be 122.2835 kg/m^3 or 0.12228 g/cm^3. While mass and density values are estimates and should be treated as such due to the uncertainty and extrapolation of information in the datasets from which they were attained, both values match planetary parameters calculated through this investigation with postulates such as Kepler's Third Law, and therefore can be treated with a degree of accuracy great enough to use as evidence toward the legitimacy of this planet candidate.

This investigation combined with prior literature (Montalto *et al.* 2020; MIT 2021) provides evidence towards the elimination of the blended EB hypothesis as an explanation for difference in transit depth and the v-shaped nature of the light curves collected within this study. However, as reiterated, despite mass and density estimated a conclusive statement cannot be

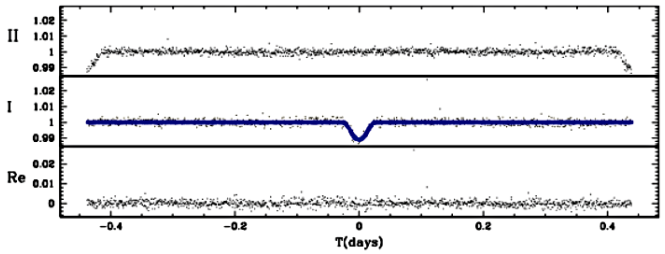

Figure 7. A transit recorded as part of a prior literature study (Montalto *et al.* 2020) shows the absence of a secondary dip common amongst blended EBs that provides greater evidence towards TOI-2341.01 existence as a hot Jupiter.

Table 8. All calculated planetary parameters for TOI-2341.01.

Planetary Parameters	*Values*	*SEM*	*Error (%)*
TOI-2341.01 radius (km)	86409	± 6011	6.957
TOI-2341.01 radius (R_E)	13.548	± 0.942	6.957
TOI-2341.01 radius (R_J)	1.209	± 0.084	6.957
Semi-major axis (KM)	1770692	± 109614	6.190
Semi-major axis (AU)	0.0118	± 0.0007	6.190
Transit duration (min)	93.6	± 8.6	9.259
Transit duration (h)	1.56	± 0.14	9.259
Transit duration (days)	0.065	± 0.006	9.259
Transit depth	4.191	± 0.529	12.614
Orbital period (days)	0.877640	± 0.000008	8.8×10^{-4}
Orbital period (h)	21.0634	± 0.0001	8.8×10^{-4}
Orbital period (min)	1263.8043	± 0.0011	8.8×10^{-4}
Mid-transit time (BJD_TDB)	2459411.742011	± 0.000131	1.0×10^{-8}
Grazing criterion	0.99	± 0.14	14.14
Planet mass (M_E) (estimate-TFOP)	55.3	N/a	n/a
Planet mass (M_J) (estimate-TFOP)	0.1739503	N/a	n/a
Planet density (kg/m^3) (estimate)	122.2835	N/a	n/a
Planet density (g/cm^3) (estimate)	0.12228	N/a	n/a

made as part of this paper due to the absence of radial velocity measurements, and hence true mass values for TOI-2341.01 and TOI-2341. Further investigations as detailed in section 8 should focus on the collection of radial velocity measurements to conclusively determine the nature of this planet candidate.

However, it can be stated with certainty that this investigation clears the field of view observed by both telescopes utilized in the imaging process of eclipsing binaries, as no false positive transits or erroneous dips have been recorded within the phase of TOI-2341.01's orbit studied during this investigation. Field-of-view measurements for both telescopes can be obtained in section 2. It can also be stated that the agreement between projected mass values and the data collected in this investigation lends significant weight toward the legitimacy of this planet candidate.

6. Results

In summary, Table 8 contains all calculated planetary and orbital parameters for TOI-2341.01 as part of this investigation. These are derived from the EXOTIC output values found in Table 4 and the ephemeris fitter output values found in Table 5. High error-values presented within transit duration can be explained by the near grazing nature of TOI-2341.01, which reduces EXOTIC's ability to determine a transit duration accurately. However, this transit duration can be visually confirmed via analysis of Figure 3, where 93 minutes is equivalent to the period of phase between –0.04 and +0.04 on the plot. Estimated values for planetary mass and density have also been provided in this table, however, it is notable that these estimates should be treated as such and do not substitute for further studies into the true mass value of this candidate planet described in section 8.

7. Conclusion

This paper presents 24 new light curves of TOI-2341.01 from observations conducted at the ELTHAM College, Cerro Tololo, and Siding Springs Observatories. These 24 new light curves and subsequent checks for the existence of nearby eclipsing binaries support the possibility of TOI-2341.01's existence as a planetary body first identified by NASA's TESS satellite. Furthermore, utilization of EXOTIC (Zellem *et al.* 2020) produced planetary parameters that were reduced via the process of standard deviation for TOI-2341.01. This investigation determined that TOI-2341.01 has a radius of 86,409 km ± 6011 km, or 1.209 R_{Jup} ± 0.084 R_{Jup}, and a semi-major axis 0.0118 AU ± 0.0007 AU, or 1,763,246 ± 58302 km. TOI-2341.01 has a revised transit depth of 4.191% ± 0.529%, with a transit duration of 0.065 ± 0.006 day (1.56 ± 0.14 hours or 93.6 ± 8.6 minutes). A revised orbital period for TOI-2341.01 was calculated to be 0.8776386 ± 0.0000042 day. The mid-transit point was revised and calculated as BJD_TDB 2459411.742011 ± 0.000131. These updated parameters demonstrate that TOI-2341.01 is larger and orbiting closer to TOI-2341 than stated in previous literature (Montalto *et al.* 2020). Furthermore, the calculated grazing criterion value of 0.99 ± 0.14 indicates that TOI-2341.01 is likely a near-grazing transit. It is also of note that estimate mass values were attained via the TESS Follow-up Observation Program that listed TOI-2341.01's mass as 55.3 M_E (0.173 M_J) (MIT 2021), and thus an estimate of planetary density, combining the mass values provided by TFOP and radius and volume values calculated in this survey, was calculated to be 122.28 kg/m^3 ± 0.12228 g/cm^3. The host star TOI-2341 is likely an M-type main-sequence star, based on TOI 2341's radius of 0.62 $R_\odot$ ± 0.02 $R_\odot$, effective temperature of 3495 K ± 157 K, a measured magnitude of 12.722 ± 0.008 in the Cousins I band (Barclay 2022) and has a calculated luminosity of 0.051 ± 0.006 given by the Stefan-Boltzmann equation (Equation 2). Furthermore, the TESS Follow-up Observation Program (TFOP) lists an estimated mass for TOI-2341 as 0.6 $M_\odot$. It can be stated that given available data collected as part of this investigation, there is significant credibility to the conclusion of TOI-2341.01's existence as a planetary body rather than a false positive. In this event TOI-2341.01 would fit the classification of a hot Jupiter or more specifically a "puffy planet." This study has determined that the field of view captured by telescopes utilized in this investigation is clear of eclipsing binaries. However, further work is required to determine TOI-2341.01's true nature, most prominently in the collection of radial velocity measurements detailed in section 8. Investigations of this kind would rule out the possibility of an eclipsing binary and add further evidence to support the existence of this candidate planet.

8. Future work

There is a strong case for continued study of the TOI-2341 system utilizing larger telescopes to obtain radial velocity measurements. While mass values have been provided by the TESS Follow-up Observation Program, these values are estimates calculated utilizing available TESS data and are not substitutes for actual values, thus they should be treated as projections. Data on the radial velocity of TOI-2341.01 and TOI-2341 would allow for the calculation of true masses for both bodies in the system, either concluding or refuting TOI-2341.01's existence as a planetary body with a much greater degree of certainty.

Future investigations into the nature of TOI-2341.01 should also conduct more transit observations, narrowing down parameters provided in both prior literatures and this paper to gain a greater insight into the TOI-2341 system as a whole. Given uncertainties presented as part of this study, follow up observations are a necessity to produce quality light curves of this exoplanet.

9. Acknowledgements

Thank you to Kalée Tock, who not only provided her insight during various discussions regarding the nature of TOI-2341.01 but also provided the programs required for the production of updated and revised mid-transit times.

Thank you to Pat Boyce for his discussion and insight into the production of this paper throughout the investigation process, allowing the team to approach the investigation process from a new perspective.

Thank you to Kyle Pearson for his assistance with issues that arose during the use of the EXOTIC software and his continued support with EXOTIC and data reduction throughout the production process. Furthermore, the utilization of his ephemeris fitter allowed for calculating an orbital period and transit midpoints that would otherwise not be possible.

Thank you to Rob Zellem for his incredible assistance with EXOTIC and the conclusions of this paper. Without his help this paper would not be possible. An additional thank you for his production and maintenance of the EXOTIC software and thank you to the EXOTIC team.

This investigation would not be possible without the NASA Exoplanet Archive, owned and operated by the California Institute of Technology in collaboration with the National Aeronautics and Space Administration under the Exoplanet Exploration Program.

Furthermore, this publication uses the EXOTIC data reduction software produced by Exoplanet Watch, a citizen science project owned and operated by NASA's Jet Propulsion Laboratory. Also utilized was the program AstroSource, made to pre-reduce data for the production of light curves under investigation conditions.

References

Barclay, T. 2022, "Characteristics of the TESS space telescope," NASA High Energy Astrophysics Science Archive Research Center (HEASARC; https://heasarc.gsfc.nasa.gov/docs/tess/the-tess-space-telescope.html).

Bertin, E. 2011, in *Astronomical Data Analysis Software and Systems XX*, eds. I. N. Evans, A. Accomazzi, D. J. Mink, A. H. Rots, ASP Conf. Ser. 442, Astronomical Society of the Pacific, San Francisco, 435.

Borucki, W. J., *et al.* 2010, *Science*, **327**, 977 (doi: 10.1126/science.1185402).

Brown, T. M., *et al.* 2013, *Publ. Astron. Soc. Pacific*, **125**, 1031.

Fitzgerald, M. T. 2018, *Robotic Telesc., Student Res. Education Proc.*, **1**, 343 (doi: 10.32374/rtsre.2017.033).

Fitzgerald, M., Gomez, E., Salimpour, S., Singleton, J., and Wibowo, R. 2021, *J. Open Source Software*, **6**, 2641 (doi: 10.21105/joss.02641).

Fowler, M. J. F., Sienkiewicz, F. F., Zellem, R. T., and Dussault, M. E. 2021, *J. British Astron. Assoc.*, **131**, 359 (arXiv:2007.13381).

Hartman, J. D., *et al.* 2011, *Astrophys. J.*, **742** (doi: 10.1088/0004-637X/742/1/59).

Lillo-Box, J., Barrado, D., Santos, N. C., Mancini, L., Figueira, P., Ciceri, S., and Henning, Th. 2015, *Astron. Astrophys.*, **577A**, 105 (doi.org/10.1051/0004-6361/201425428).

Mancini, L., *et al.* 2014, *Astron. Astrophys.*, **568A**, 127 (doi: 10.1051/0004-6361/201424106).

Mandushev, G., *et al.* 2007, *Astrophys. J.*, **667**, L195 (doi: 10.1086/522115).

Massachusetts Institute of Technology. 2021, TESS Followup Observation Program, TOIs accessed 2021-11-11 (https://tess.mit.edu/wp-content/uploads/RVvaluesByESM_onlyPCs_rankedESM.txt).

Montalto, M., *et al.* 2020, *Mon. Not. Roy. Astron. Soc.*, **498**, 1726 (doi: 10.1093/mnras/staa2438).

Pearson, K. A. 2019, *Astron. J.*, **158**, 243 (doi: 10.3847/1538-3881/ab4e1c).

Ricker, George R., *et al.* 2015, *J. Astron. Telesc. Instrum. Syst.*, **1**, 014003 (doi: 10.1117/1.JATIS.1.1.014003).

Salimpour, S., Fitzgerald, M., and Demmert, H. 2021, *Astron. Theory, Obs. Methods*, **2**, 45 (doi: 10.32374/atom.2020.2.6).

Sarva, J., Freed, R., Fitzgerald, M. T., and Salimpour, S. 2020, *Astron. Theory, Obs. Methods*, **1**, 34.

Torres, G., *et al.* 2010, *Astrophys. J.*, **715**, 458 (doi: 10.1088/0004-637X/715/1/458).

Wang, J., Fischer, D. A., Horch, . P., and Huang, X. 2015, *Astrophys. J.*, **799**, 229 (doi: 10.1088/0004-637X/799/2/229).

Zellem, Robert T., *et al.* 2020, *Publ. Astron. Soc. Pacific*, **132**, 054401 (doi: 10.1088/1538-3873/ab7ee7).

Appendix A: Light curves of TOI-2341.01 reduced by EXOTIC.

The appendix is a complete collection of all transits observed as part of this investigation into the nature of TOI-2341.01. Light curve designations are listed below their respective plot, and further details are attributed to their designations in Table 2.

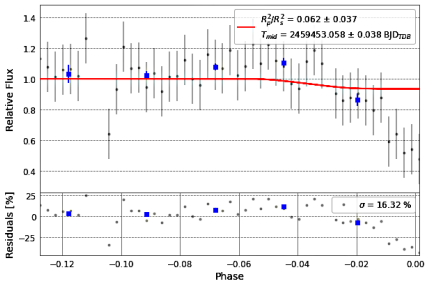

TOI2341.01ECB.1

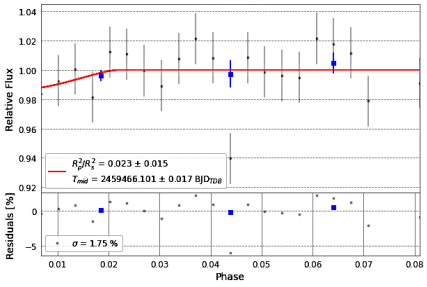

TOI2341.01ECIP.1

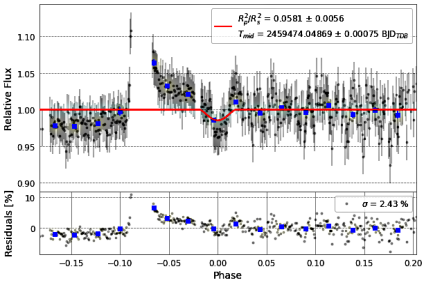

TOI2341.01ECL.1

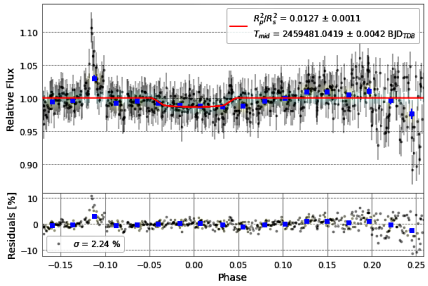

TOI2341.01ECL.2

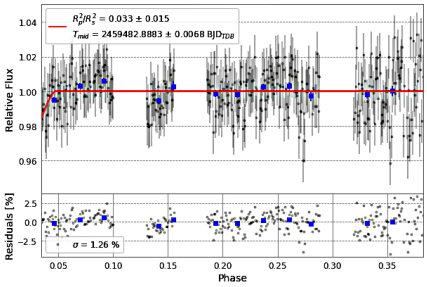

TOI2341.01ECL.3

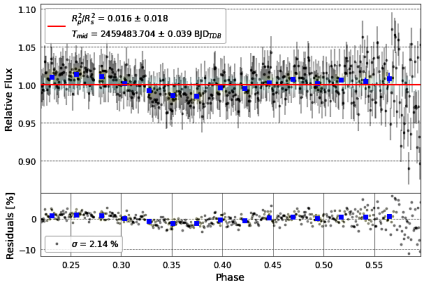

TOI2341.01ECL.4

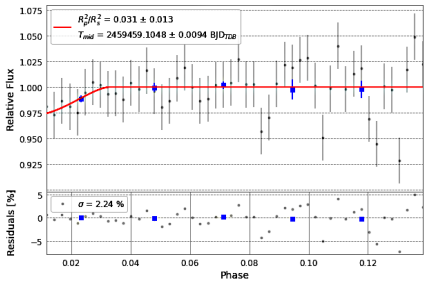

TOI2341.01ECRP.1

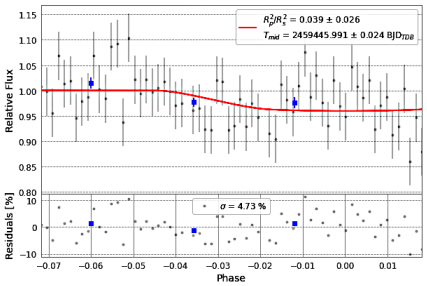

TOI2341.01ECRP.2

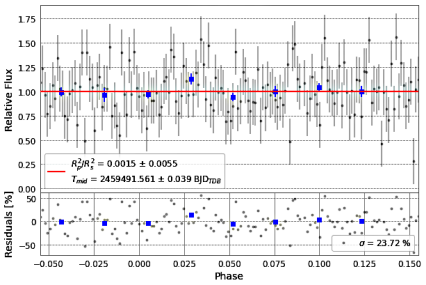

TOI2341.01LCOB.1

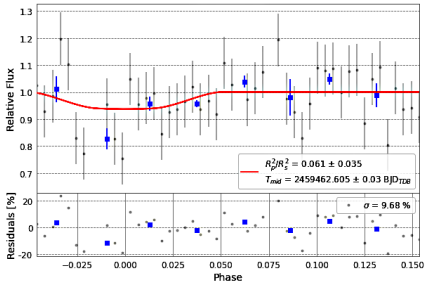

TOI2341.01LCOB.2

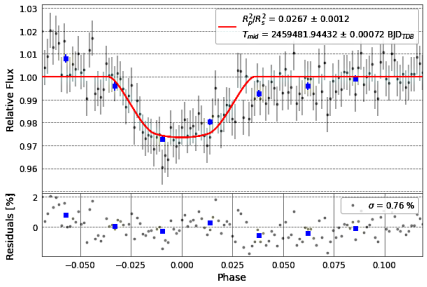

TOI2341.01LCOIP.1

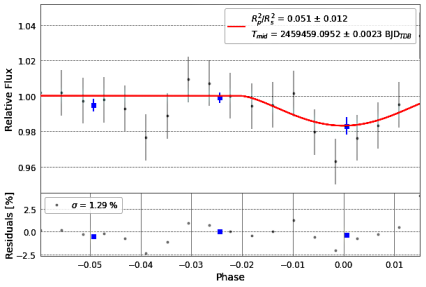

TOI2341.01LCOIP.2

Appendix A: Light curves of TOI-2341.01 reduced by EXOTIC (cont.).

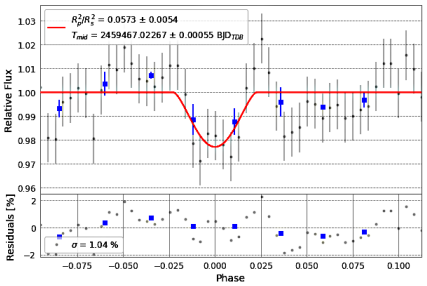

TOI2341.01LCOIP.3

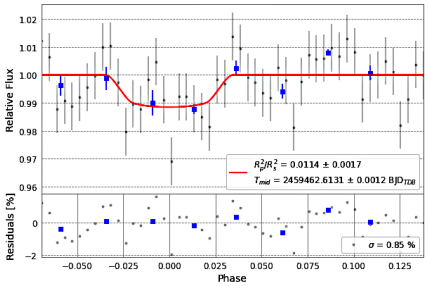

TOI2341.01LCORP.1

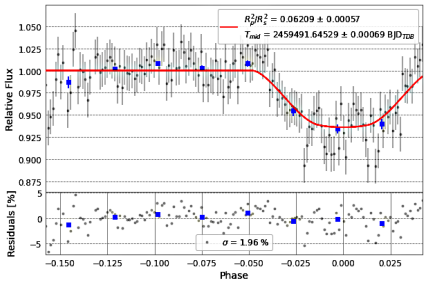

TOI2341.01LCORP.2

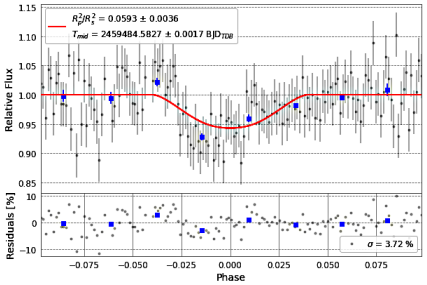

TOI2341.01LCOV.1

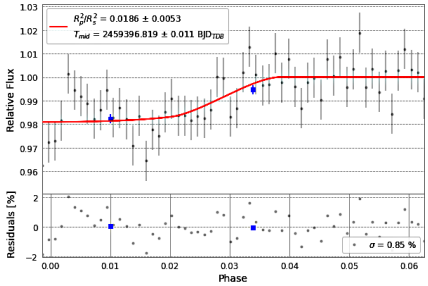

TOI2341.01LCOW.1

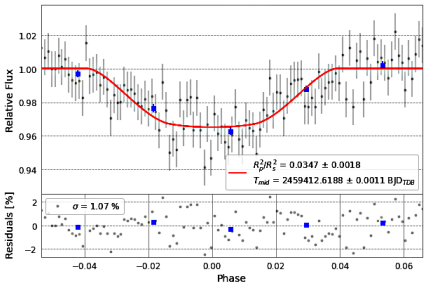

TOI2341.01LCOW.2

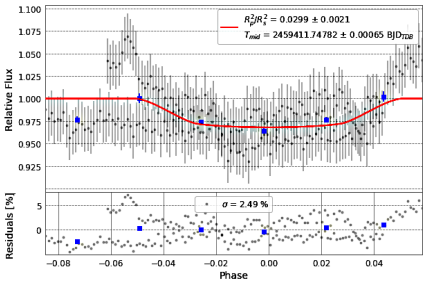

TOI2341.01LCOW.3

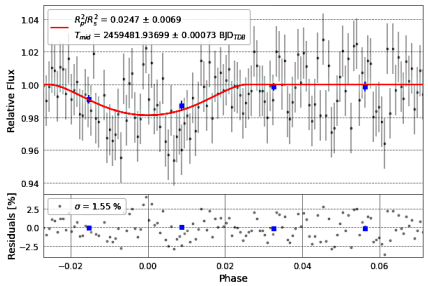

TOI2341.01LCOW.4

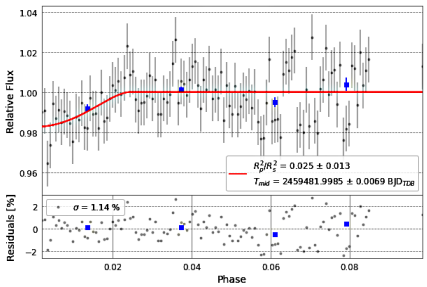

TOI2341.01LCOW.5

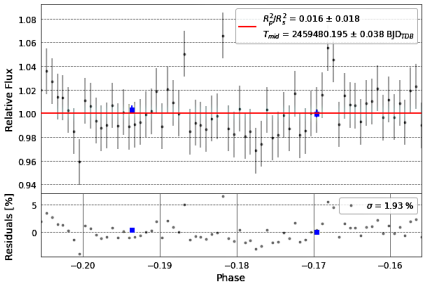

TOI2341.01LCOW.6

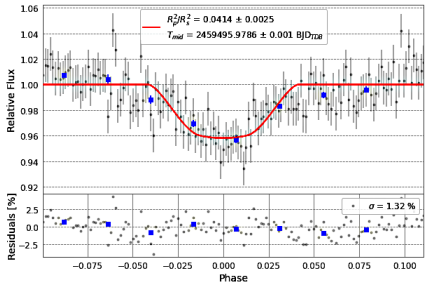

TOI2341.01LCOZS.1

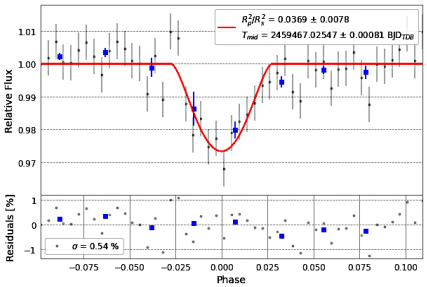

TOI2341.01LCOZS.2